Recent results on 4-body, charm semileptonic decays

Jim Wiss

University of Illinois, 1110 W. Green, Urbana IL , 61801

We summarize recent data on 4-body charm semileptonic decay concentrating on $D_s^+ \rightarrow K^+ K^- e^+ \nu$ and $D^+ \rightarrow K^- \pi^+ \ell^+ \nu$. We begin with giving some motivation for the study of these decays. We discuss several of the models traditionally used to describe these decays and conclude by presenting a non-parametric analysis of $D^+ \rightarrow K^- \pi^+ e^+ \nu$ and its possible extension into non-parametric studies of $D^+ \rightarrow K^- \pi^+ \mu^+ \nu$.

I. INTRODUCTION

Figure 1 shows a cartoon of the $D^0 \rightarrow K^- \ell^+ \nu$ decay process. All of the hadronic complications for this process is contained in q^2 dependent form factors that are computable using non-perturbative methods such as LQCD. Although semi-leptonic process can in principle provide a determination of charm CKM elements, one frequently uses the (unitarity constrained) CKM measurements, lifetime, and branching fraction to measure the scale of charm semileptonic decay constants and compare them to LQCD predictions. The q^2 dependence of the semileptonic form factor can also be directly measured and compared to theoretical predictions.

The hope is that charm semileptonic decays can provide high statistics, precise tests of LQCD calculations and thus validate the computational techniques for charm. Once validated, the same LQCD techniques can be used in related calculations for B-decay and thus produce CKM parameters with significantly reduced theory systematics.
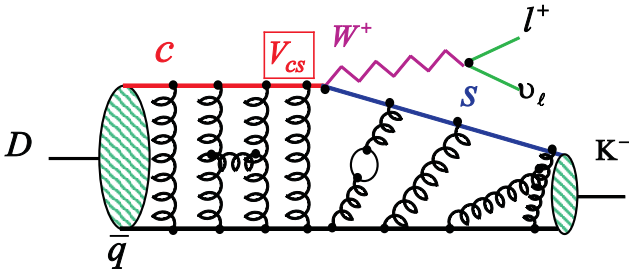

FIG. 1: Diagrams for the semileptonic decay of charmed mesons. The hadronic,QCD complications are contained in q^2 dependent form factors.

Although recent, unquenched LQCD calculations are unavailable for $D \rightarrow$ vector $\ell^+ \nu$ processes, owing to the instability of the vector parent, I hope that the 4-body will provide additional tests of LQCD for a variety of spin states which will further help calibrate the lattice, and provide confidence in analogous decays for the beauty sector.

I find it remarkable that 4-body semileptonic decays such as $D_s^+ \rightarrow K^+ K^- \ell^+ \nu$ and $D^+ \rightarrow K^- \pi^+ \mu^+ \nu$

are so heavily dominated by the vector decays $D_s^+ \rightarrow \phi \, e^+ \nu_e$ and $D^+ \rightarrow \overline{K}^{*0} \mu^+ \nu$. Figure 2 illustrates this dominance by showing data from FOCUS[1] and recent data from BaBar[2]. The absence of a substantial
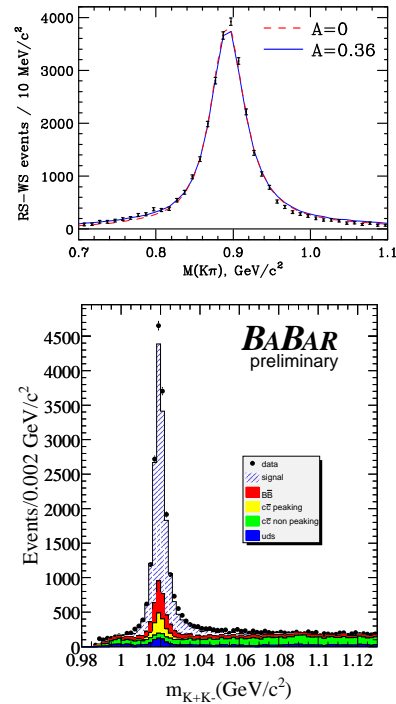

FIG. 2: We show the $m(K^+ K^-)$ spectra obtained in $D_s^+ \rightarrow K^+ K^- \ell^+ \nu$ by BaBar[2] and $m(K^- \pi^+)$ by FOCUS[1]. The curve on the FOCUS $m(K^- \pi^+)$ spectra is a $\overline{K}^{*0}$ line shape both with (A = 0.36) and without (A = 0) a small s-wave, non-resonant component which was found through an interference in the decay intensity and is described later. The $m(K^+ K^-)$ spectra obtained by BaBar is very strongly dominated by the ϕ resonance along with a few known backgrounds.

non-resonant, or higher spin resonance component to these decays means the decay angular distribution can be described in terms of three, q^2-dependent helicity basis form factors that describe the coupling of the lepton system to the three helicity states of the vector meson according to Eq. (1) :

$$|\mathcal{A}|^2 \approx \frac{q^2}{8} \left| \begin{array}{c} (1+\cos\theta_l)\sin\theta_V e^{i\chi} H_+(q^2) \\ -(1-\cos\theta_l)\sin\theta_V e^{-i\chi} H_-(q^2) \\ -2\sin\theta_l \cos\theta_V H_0(q^2) \end{array} \right|^2 \quad (1)$$

The three decay angles describing the $D^+ \to K^-\pi^+\ell^+\nu$ decay, referenced in Eq.(1), are illustrated by Fig. 3.
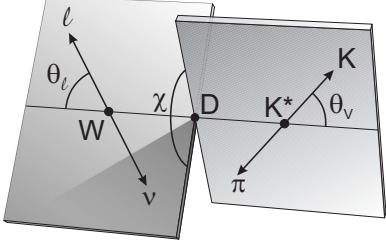

II. ANALYTIC MODELS FOR FORM FACTORS

We begin by describing the three form factors relevant to $D \to$ vector $\ell^+\nu$ although there is strong evidence [1][3] for a non-resonant, s-wave component to $D^+ \to K^-\pi^+\ell^+\nu$. A new, fifth form factor $H_T(q^2)$ is also required for $D^+ \to \overline{K}^{*0}\mu^+\nu$ to describe the suppressed coupling of the $\overline{K}^{*0}$ to a left-handed μ^+.

The $H_+(q^2)$, $H_-(q^2)$, $H_0(q^2)$ form factors are linear combinations of two axial and one vector form factor [5] according to Eq. (2):

$$\begin{aligned} H_\pm(q^2) &= (M_D + m_{K\pi})A_1(q^2) \mp 2\frac{M_D K}{M_D + m_{K\pi}}V(q^2), \\ H_0(q^2) &= \frac{1}{2m_{K\pi}\sqrt{q^2}}\left[(M_D^2 - m_{K\pi}^2 - q^2)(M_D + m_{K\pi})A_1(q^2) - 4\frac{M_D^2 K^2}{M_D + m_{K\pi}}A_2(q^2)\right] \end{aligned}$$

$$(2)$$

where K is the momentum of the $K^-\pi^+$ system and $m_{K\pi}$ is its mass.

Eq.(3) provides considerable insight into the expected analytic form for semileptonic form factors. It uses a dispersion relation obtained using Cauchy's Theorem under the assumption that a form factor is an analytic, complex function apart from some known singularities. Fig. 4 illustrates the Cauchy's Theorem contour for the case for the $f_+(q^2)$ form factor describing $D^0 \to K^-\ell^+\nu$.

The form factor singularities will consist of a sum of simple poles at the D meson -kaon vector bound states (e.g. D_s^{*+}) plus a cut beginning at the $D-$kaon continuum in the cross process: $\nu\ell^+ \to D$ kaon. The dispersion relation gives the form factor $(F(q^2))$ as a sum over the spectroscopic poles plus an integral over the cut.

$$F(q^2) = \frac{\mathcal{R}}{m_{D_s^*}^2 - q^2} + \frac{1}{\pi}\int_{(m_D+K)^2}^\infty \frac{\text{Im}\{f_+(s)\}}{s - q^2 - i\varepsilon}ds \quad (3)$$

Both the cuts and poles are generally beyond the physical q^2_{max} and thus can never be actually realized.

Spectroscopic pole dominance (SPD) was an early parameterization for the form factors relevant to both $D \to$ vector $\ell^+\nu$ and $D \to$ pseudoscalar $\ell^+\nu$. SPD ignores the cut integral entirely and approximates $F(q^2)$ using just the first term of Eq.(3). The advantage of
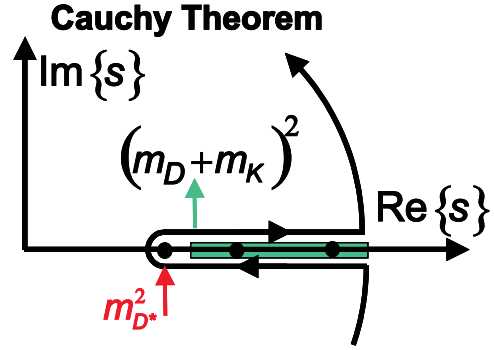
FIG. 3: Definition of kinematic variables.

FIG. 4: Each form factor is assumed to be an analytic function with pole singularities at the masses of bound states, and cuts that start at the start of the continuum. We illustrate the case of $D^0 \to K^-\ell^+\nu$. One can use Cauchy's theorem with the indicated contour to write an dispersion expression for each form factor in the physical range $0 < q^2 < (m_D - m_K)^2$

SPD approach is that it requires only a single unknown fitting parameter $\mathcal{R}$ to describe each $F(q^2)$ since the positions of the bound states are well known. SPD entirely predicts *shape* of $D \to$ pseudoscalar $\ell^+\nu$ decay intensity and predicts that the *shape* for the

$D^+ \to \overline{K}^{*0}\ell^+\nu_\ell$ can be fit by just two parameters which are traditionally taken to be the axial and vector form factor ratios at $q^2 = 0$: $r_v = V(0)/A_1(0)$ and $r_2 = A_2(0)/A_1(0)$.

BaBar [2] has recently published an interesting SU(3) test based on SPD applied to $D_s^+ \to \phi\, e^+\nu_e$. Figure 5 compares the r_v and r_2 parameters measured for $D_s^+ \to \phi\,\ell^+\nu_\ell$ to those previously measured for $D^+ \to \overline{K}^{*0}\ell^+\nu_\ell$. By SU(3) symmetry and explicit calculation, the r_v and r_2 form factor ratios for $D^+ \to \overline{K}^{*0}\ell^+\nu_\ell$ and $D_s^+ \to \phi\,\ell^+\nu_\ell$ decays are expected to be very close to each other. This is true for r_v, but previous to the recent measurement by the FOCUS Collaboration[6], r_2 for $D_s^+ \to \phi\,\ell^+\nu_\ell$ was measured to be roughly a factor of two larger than that for $D^+ \to \overline{K}^{*0}\ell^+\nu_\ell$. BaBar[2] has confirmed the expected consistency between the form factor ratios obtained for $D_s^+ \to \phi\,\ell^+\nu_\ell$ and $D^+ \to \overline{K}^{*0}\ell^+\nu_\ell$ with unparalleled statistics.

FIG. 6: Effective pole mass measurement in $D^0 \to K^- e^+ \nu$ over the years. The green line is the $m_{D_S^*}$ spectroscopic pole mass and is inconsistent with the average of the displayed data by 5.1 σ.

that effective pole is significantly lower than the spectroscopic pole, underscoring the importance of the cut integral contribution for this decay.
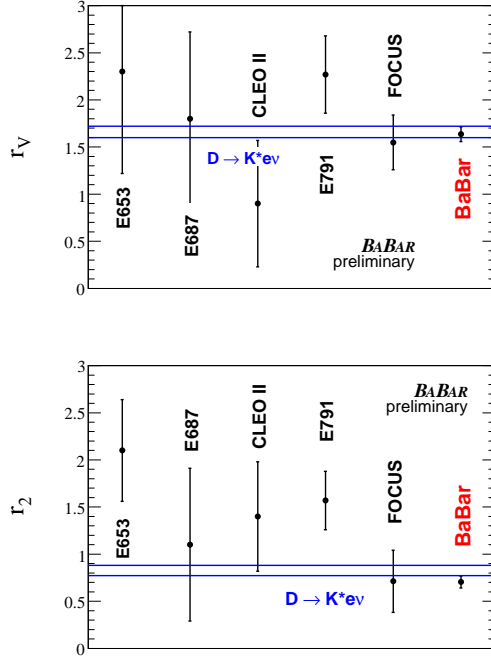

FIG. 7: Illustration of Hill transformation approach.

FIG. 5: The r_v and r_2 form factor ratios measured for $D_s^+ \to \phi\,\ell^+\nu_\ell$ by various experiments. The blue lines show $\pm 1\sigma$ bands for the weighted average of the $D^+ \to \overline{K}^{*0}\ell^+\nu_\ell$ form factor ratios compiled in Reference [4]. It is expected from SU(3) symmetry that the $D_s^+ \to \phi\,\ell^+\nu_\ell$ form factors should be very close to those for $D^+ \to \overline{K}^{*0}\ell^+\nu_\ell$

Several experiments have tested SPD by measuring an "effective" pole mass (m_{pole})in $D^0 \to K^- e^+ \nu$ decay where the pole mass is defined using $f_+(q^2) \propto 1/(m_{pole}^2 - q^2)$. As Fig. 6 from Reference [4] shows, as errors have improved over the years, it becomes clear
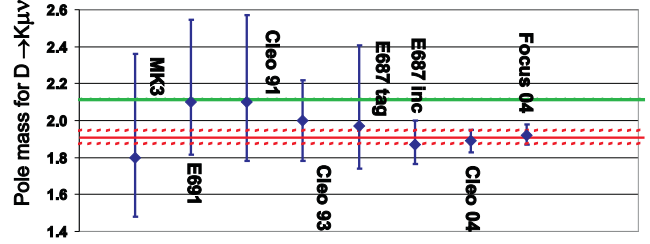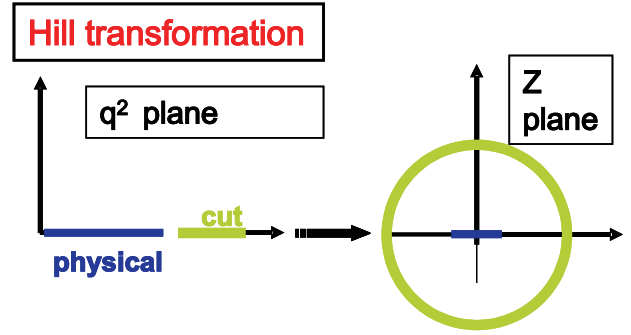
Several parameterizations have been proposed to include the cut integral in Eq. (3) as well as the spectroscopic poles. Becirevic and Kaidalov (1999) [7] proposed a new parameterization for the $D \to$ pseudoscalar $\ell^+\nu$ for factor $f_+(q^2)$ that replaces the cut integral by an effective pole where the heavy quark symmetry and other theoretical ideas are used to relate the residue and effective pole position. These constraints leads to a modified pole form with a single additional parameter α that describes the degree to which the single spectroscopic pole fails to match $f_+(q^2)$ for a given process.

$$f_+(q^2) = \frac{f_+(0)}{\left(1 - q^2/m_{D*}^2\right)\left(1 - \alpha q^2/m_{D*}^2\right)} \qquad (4)$$

S. Fajfer and J. Kamenik [8] have recently extended the effective pole approach to the three helicity form factors relevant to $D \to$ vector $\ell^+\nu$ decays.

R.J. Hill[9][10] has proposed an alternative way of viewing form factors which is illustrated in Fig. 7. The basic idea is to devise a transformation of a form factor from the complex q^2 plane to a complex z plane.

This transformation is devised to (1) remove the spectroscopic poles and (2) put the cuts far away from the physical z region. After the transformation, since the singularities have been removed or diminished, each form factor can be well represented by a low order Taylor series in z. The transformation approach is known[10] to work very well in B-decays where the physical q^2 region gets very close to the singularities for pseudo-scalar B semileptonic decay. It also works well for pseudoscalar charm pseudoscalar semileptonic decay[9].

III. $D^+ \to K^-\pi^+\ell^+\nu$ DECAYS

Although historically $D^+ \to \overline{K}^{*0}\ell^+\nu_\ell$ have been the most accessible semileptonic decays in fixed target experiments owing to their ease of isolating a signal, they are significantly more complicated to analyze than $D \to$ pseudoscalar $\ell^+\nu$. One problem is that a separate helicity form factor is required for each of the three helicity states of vector meson. The q^2 dependence of these form factors cannot be simply measured from the q^2 dependence of the decay rate as is the case in $D \to$ pseudoscalar $\ell^+\nu$ but rather must be entangled from the q^2 dependence of the angular distribution such as that given by Eq. (1).

Another complication is that since $D^+ \to K^-\pi^+\ell^+\nu$ states result in a multihadronic final state, the $D^+ \to \overline{K}^{*0}\ell^+\nu_\ell$ final states can potentially interfere with $D^+ \to K^-\pi^+\ell^+\nu$ processes with the $K^-\pi^+$ in various angular momentum waves with each wave requiring its own form factor. Because the $m_{K\pi}$ distribution in $D^+ \to K^-\pi^+\ell^+\nu$ was an excellent fit to the $\overline{K}^{*0}$ Breit-Wigner as shown in Fig. 2, it was assumed for many years that any non-resonant component to $D^+ \to K^-\pi^+\ell^+\nu$ must be negligible. In

2002, FOCUS observed a strong, forward-backward asymmetry in $\cos\theta_V$ for events with $m_{K\pi}$ below the $\overline{K}^{*0}$ pole with essentially no asymmetry above the pole as shown in Figure 8. The simplest explanation for this asymmetry is the presence of a linear $\cos\theta_V$ term in the decay intensity due to interference between the $D^+ \to \overline{K}^{*0}\mu^+\nu$ and a non-resonant, s-wave amplitude. This interference is the second-to-last term in Eq. (5), which is basically an expanded out version of Eq. (1), integrated over acoplanarity χ. We also explicitly include the $\overline{K}^{*0}$ Breit-Wigner amplitude (BW). Note that all other interference terms (such as a possible $H_+(q^2) \times H_-(q^2)$ contribution) vanish because of the $\int_0^{2\pi} d\chi \exp(i\Delta\chi)$ integration. Only "same" helicity contributions can interfer in the acoplanarity averaged intensity. We will argue shortly that an appropriate δ can create the asymmetry pattern shown in Fig. 8

Finally we introduce an additional form factor ($h_0(q^2)$) in Eq. (5) to describe the coupling to the
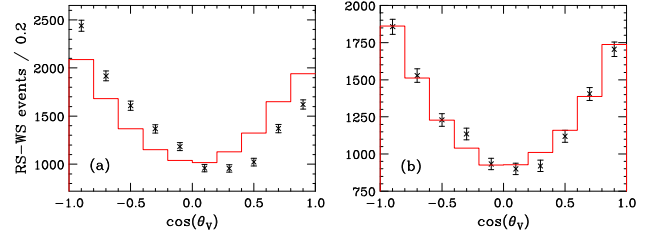

FIG. 8: Evidence for s-wave interference in $D^+ \to K^-\pi^+\ell^+\nu$.

s-wave amplitude.

$$\int |\mathrm{A}|^2 \, d\chi = \frac{1}{8}q^2 \left\{ \begin{array}{l} ((1+\cos\theta_l)\sin\theta_V)^2 \left|H_+(q^2)\right|^2 |BW|^2 \\ + ((1-\cos\theta_l)\sin\theta_V)^2 \left|H_-(q^2)\right|^2 |BW|^2 \\ + (2\sin\theta_l\cos\theta_V)^2 \left|H_0(q^2)\right|^2 |BW|^2 \\ + 8\left(\sin^2\theta_l\cos\theta_V\right) H_0(q^2)h_o(q^2)\mathrm{Re}\left\{Ae^{-i\delta}BW\right\} \\ + O(A^2) \end{array} \right\} \tag{5}$$

A.   Asymtotic Forms

Assuming that $A_{1,2}(q^2)$ and $V(q^2)$ approach a constant in the low q^2 limit, as expected in spectroscopic pole dominance, Eq. (2) shows $q^2 \to 0$, both $H_+(q^2)$ and $H_-(q^2)$ approach a constant as well. By way of constrast, $H_0(q^2)$ will diverge in the low q^2 limit according to Eq. (2) owing to the $1/\sqrt{q^2}$ prefactor.

Since the helicity intensity contributions are proportional to $q^2 H_\pm^2(q^2)$, according to Eq.(5), the $H_\pm$ intensity contributions vanish in this limit, while $q^2 H_0^2(q^2)$ will approach a constant.

Figure 9 expains why this is true. As $q^2 \to 0$, the e^+ and ν become collinear with the virtual W^+. For $H_+(q^2)$ and $H_-(q^2)$, the virtual W^+ must be in the $|1,\pm1\rangle$ state which means that the e^+ and ν must

both appear as either right-handed or left-handed thus violating the charged current helicity rules. Hence $q^2 H_\pm(q^2)$ vanishes at low q^2. For $H_0(q^2)$, the W^+ is in $|1,0\rangle$ state thus allowing the e^+ and ν to be in their (opposite) natural helicity state. Hence at low q^2, $q^2 H_0(q^2) \to$ constant which allows for $D^+ \to \overline{K}^{*0} \mu^+ \nu$ decays as $q^2 \to 0$. Presumably $h_0(q^2) \to 1/\sqrt{q^2}$ as well since it also describes a process with W^+ in the $|1,0\rangle$ state
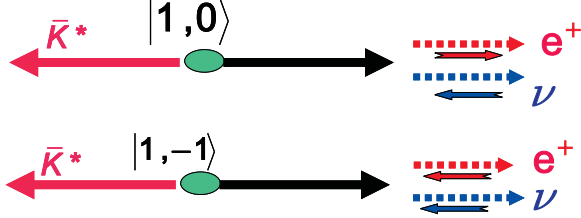

FIG. 9: The electron helicity state in the low q^2 limit. When the virtual W^+ is in the zero helicity state, the e^+ and ν have the opposite helicity and can be in their charged-current helicity states. When the virtual W^+ is in the $|1,\pm 1\rangle$ state the e^+ and ν must be in the same helicity states and violate the weak helicity rules.

Here is a final observation on the expected asymptotic behavior of the helicity form factors. As $q^2 \to q^2_{\max}$, the momenta of the virtual W^+ and $\overline{K}^{*0}$ approaches zero and θ_V and θ_ℓ can no longer be defined. This means the $D^+ \to \overline{K}^{*0} \ell^+ \nu_\ell$ decay must be isotropic and Eq. (5) implies that $|H_\pm|^2 \to |H_0|^2$ as $q^2 \to q^2_{\max}$. A spectroscopic pole dominance model for the axial and vector form factors will automatically satisfies these asymtotic limits according to Eq.(2).

IV. PROJECTION WEIGHTING TECHNIQUE

We next describe the projective weighting technique that we use to extract the helicity basis form factors.

This technique was initially developed by the FOCUS Collaboration[13] and applied to CLEO[3] data. As shown in Eq. (5), after integrating over acoplanarity, the decay intensity is just a sum over four terms that consist of a form factor product times a characteristic angular distribution in θ_V and θ_ℓ. The acoplanarity integration has significantly simplified the problem by eliminating the five of the possible six interference terms between the four form factor amplitudes with different helicities. We begin by making a binned version of Eq. (5) given by Eq. (6), where for simplicity we only write three of the terms.

$$\vec{D}_i = f_+(q_i^2)\,\vec{m}_+ + f_-(q_i^2)\,\vec{m}_- + f_0(q_i^2)\,\vec{m}_0 \quad (6)$$

We use 25 joint $\Delta \cos\theta_V \times \Delta \cos\theta_\ell$ angular bins: 5 evenly spaced bins in $\cos\theta_V$ times 5 bins in $\cos\theta_\ell$ and 6 bins in q^2 ($i = 0 \to 6$). The number of $D^+ \to K^- \pi^+ \ell^+ \nu$ events observed in each of the 25 angular bins is packed into a twenty-five component $\vec{D}_i$ "data" vector.

The $f_\pm(q_i^2)$ and $f_0(q_i^2)$ are proportional to $H_\pm^2(q^2)$, $H_0^2(q^2)$ averaged over the q_i^2 bin along with all phase space and efficiency factors. The $\vec{m}_\pm$ and $\vec{m}_0$ are the angular distributions due to each individual form factor product packed into a 25-vector for each of the six q^2 bins. The acceptance and phase space corrected m-vectors are obtained directly from a Monte Carlo simulation where a given form factor product is turned on and all others are turned off. We can write Eq. (6) as the "component equation" shown in Eq. (7) by forming the dot product with each of the three m-vectors:

$$\begin{pmatrix} \vec{m}_+ \cdot \vec{D}_i \\ \vec{m}_- \cdot \vec{D}_i \\ \vec{m}_0 \cdot \vec{D}_i \end{pmatrix} = \begin{pmatrix} \vec{m}_+ \cdot \vec{m}_+ & \vec{m}_+ \cdot \vec{m}_- & \vec{m}_+ \cdot \vec{m}_0 \\ \vec{m}_- \cdot \vec{m}_+ & \vec{m}_- \cdot \vec{m}_- & \vec{m}_- \cdot \vec{m}_0 \\ \vec{m}_0 \cdot \vec{m}_+ & \vec{m}_0 \cdot \vec{m}_- & \vec{m}_0 \cdot \vec{m}_0 \end{pmatrix} \begin{pmatrix} f_+(q_i^2) \\ f_-(q_i^2) \\ f_0(q_i^2) \end{pmatrix} \quad (7)$$

The solution to Eq. (7) can be written as:

$$f_+(q_i^2) = {}^i\vec{P}_+ \cdot \vec{D}_i \,, \ \ f_-(q_i^2) = {}^i\vec{P}_- \cdot \vec{D}_i \,, \ \ f_0(q_i^2) = {}^i\vec{P}_0 \cdot \vec{D}_i \quad (8)$$

where ${}^i\vec{P}_\alpha$ vectors are given by Eq. (9).

$$
\begin{pmatrix} {}^{i}\vec{P}_{+} \\ {}^{i}\vec{P}_{-} \\ {}^{i}\vec{P}_{0} \end{pmatrix} = \begin{pmatrix} \vec{m}_{+}\cdot\vec{m}_{+} & \vec{m}_{+}\cdot\vec{m}_{-} & \vec{m}_{+}\cdot\vec{m}_{0} \\ \vec{m}_{-}\cdot\vec{m}_{+} & \vec{m}_{-}\cdot\vec{m}_{-} & \vec{m}_{-}\cdot\vec{m}_{0} \\ \vec{m}_{0}\cdot\vec{m}_{+} & \vec{m}_{0}\cdot\vec{m}_{-} & \vec{m}_{0}\cdot\vec{m}_{0} \end{pmatrix}^{-1} \begin{pmatrix} \vec{m}_{+} \\ \vec{m}_{-} \\ \vec{m}_{0} \end{pmatrix} \qquad (9)
$$

It is useful to think of forming the dot products in Eq. (8) by making a weighted histogram:

$$
\vec{P}_{+}\cdot\vec{D} = \left[\vec{P}_{+}\right]_{1} n_{1} + \left[\vec{P}_{+}\right]_{2} n_{2} + \cdots \left[\vec{P}_{+}\right]_{25} n_{25} \quad (10)
$$

Eq. (10) demonstrates the product $\vec{P}_{+}\cdot\vec{D}$ is equivalent to weighting the n_{1} events in angular bin 1 by $\left[\vec{P}_{+}\right]_{1}$, weighting the n_{2} events in angular bin 2 by $\left[\vec{P}_{+}\right]_{2}$, etc. Hence each form factor product such as $f_{+}(q_{i}^{2})$ can be obtained by simply weighting the data by $\left[\vec{P}_{+}\right]_{i}$ where i is the angular bin of the given datum. The acceptance and phase space factors can be easily included the projective weights as well in order to directly produce each form factor product. Hence the (arbitrarily normalized) form factor products $H_{+}^{2}(q^{2})$, $H_{-}^{2}(q^{2})$, and $H_{0}^{2}(q^{2})$ can then be obtained by making three weighted histograms using the efficiency rescaled ${}^{i}\vec{P}_{+}$, ${}^{i}\vec{P}_{-}$, and ${}^{i}\vec{P}_{0}$ weights respectively.

The same, basic projective weighting approach has been recently applied by the FOCUS Collaboration[11] for a non-parametric analysis of the $K^{-}\pi^{+}$ amplitudes in the hadronic decay $D^{+} \rightarrow K^{-}K^{+}\pi^{+}$. To whet the appetite, Fig.10 shows the $K^{-}\pi+$ amplitudes obtained in that analysis. The s-wave amplitude shown in Fig. 10 (a) and begs comparison with the s-wave amplitude obtained in a K-matrix analysis[12] of $D^{+} \rightarrow K^{-}\pi^{+}\pi^{+}$ described by S. Malvezzi in these proceedings.

V. A NON-PARAMETRIC ANALYSIS OF THE HELICITY FORM FACTORS IN
$$D^{+} \rightarrow K^{-}\pi^{+}\ell^{+}\nu$$

Figure 11 shows the four weighted histograms from an analysis of 281 pb^{-1} $\psi(3770)$ CLEO data[3]. Figure 11 shows the expected behavior discussed in Section III A. In particular, $H_{\pm}q^{2} \rightarrow$ constant as $q^{2} \rightarrow 0$ while the zero-helicity form factors, $H_{0}(q^{2})$ and $h_{0}(q^{2})$, diverge as $1/\sqrt{q^{2}}$. It is interesting to note that although the non-resonant, s-wave amplitude is too small to see in the $K^{-}\pi^{+}$ mass spectrum (Fig. 2), its form factor is measured with roughly the same precision as $H_{+}^{2}(q^{2})$ or $H_{-}^{2}(q^{2})$. The curves give the helicity form factors according to Eq. (5) , using spectrocopic pole dominance and the r_{v}, r_{2}, and s-wave parameters measured by FOCUS[14]. Apart from the $h_{0}(q^{2}) H_{0}(q^{2})$ interference form factor product, the spectroscopic pole
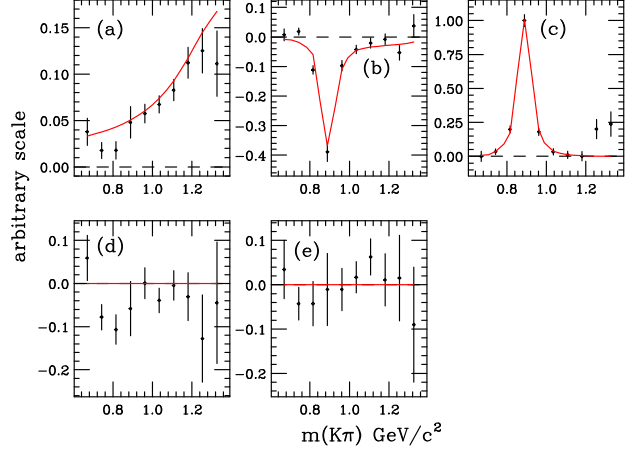

FIG. 10: Results of a non-parametric analysis[11] of $D^{+} \rightarrow K^{-}K^{+}\pi^{+}$ using a variant of the projective weighting technique described here. The plots are: (a) S^{2} $(m_{K\pi})$ direct term, (b) 2 $S(m_{K\pi}) \times P(m_{K\pi})$ interference term, (c) P^{2} $(m_{K\pi})$ direct term, (d) 2 $P(m_{K\pi}) \times D(m_{K\pi})$ interference term and (e) D^{2} $(m_{K\pi})$ direct term. The overlay is a model including the $\overline{K}^{*0}$ which dominates P^{2} $(m_{K\pi})$, and a wider $\overline{K}_{0}^{*0}(1430)$ which dominates S^{2} $(m_{K\pi})$.
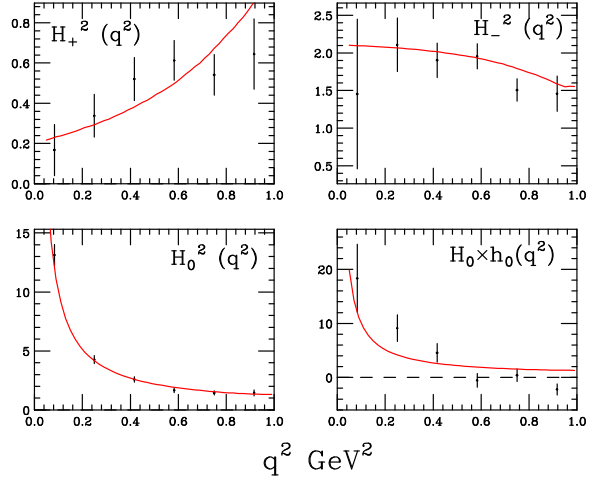

FIG. 11: The four helicity form factor products obtained using the 281 pb^{-1} data set from CLEO[3]. The curves represent the model of Reference [14].

dominance model is a fairly good match to the CLEO non-parametric analysis. This suggests that the ad-

hoc assumption, used by FOCUS, that $h_0(q^2)=H_0(q^2)$ is questionable but it will probably take more data, and some theoretical guidance, to gain insight into the nature of the discrepancy.

Figure 12 gives a different insight into the helicity basis form factors by plotting the intensity contributions of each of the form factor products. This is the form factor product multiplied by q^2. Since $q^2 H_0^2(q^2)$ dominates, we normalized form factors such that $q^2 H_0^2(q^2) = 1$ at $q^2 = 0$ but use the same scale factor for the other three form factors. As expected, both $q^2 H_+^2(q^2)$ and $q^2 H_-^2(q^2)$ rise from zero with increasing q^2 and they both appear to approach $q^2 H_0^2(q^2)$ at q^2_{max} – although $q^2 H_+^2(q^2)$ seems slightly lower than $q^2 H_0^2(q^2)$ at q^2_{max}.
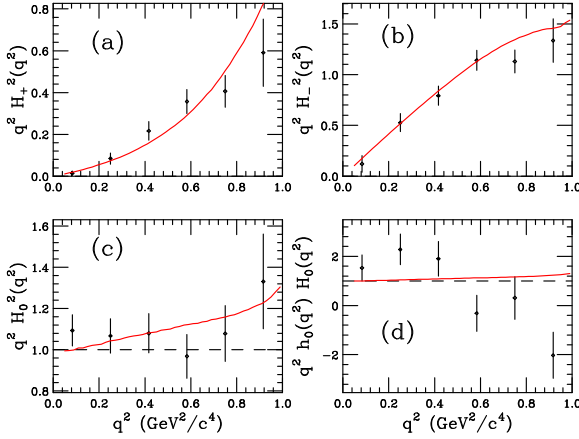

FIG. 12: Non-parametric form factor products obtained for the data sample (multiplied by q^2) The reconstructed form factor products are shown as the points with error bars, where the error bars represent the statistical uncertainties. The solid curves in the histograms represent a form factor model described in Ref. [14]. The histogram plots are: (a) $q^2 H_+^2(q^2)$, (b) $q^2 H_-^2(q^2)$, (c) $q^2 H_0^2(q^2)$, and (d) $q^2 h_0(q^2) H_0(q^2)$. The form factors are normalized such that $q^2 H_0^2(q^2) \to 1$ as $q^2 \to 0$.

What can we learn about the pole masses? Unfortunately Fig. 13 shows that the present data is insufficient to learn anything useful about the pole masses. On the left of Figure 13, the helicity form factors are compared to a model generated with the FOCUS form factor ratios[14] and the standard pole masses of 2.1 GeV for the vector pole and 2.5 GeV for the two axial poles. On the right side of Fig. 13, the form factors are compared to a model where the pole masses are set to infinity meaning that the axial and vector form factors are constant. Both models fit the data equally well.

The data of Fig. 13 is consistent with the spectroscopic pole dominance albeit with essentially no sensitivity to the pole masses. Fig. 14 shows that it is also consistent with the expected behavior under a Hill transformation, illustrated earlier in Fig. 7.
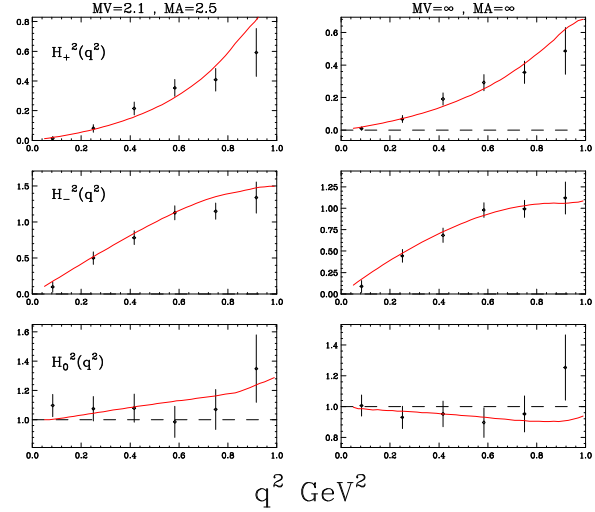

FIG. 13: Non-parametric form factor products obtained for data (multiplied by q^2) The solid curves are based on the s-wave model and measurements described in Reference [14]. The reconstructed form factor products are the points with error bars. The three plots on the right are the usual model with the spectroscopic pole masses; while the three plots on the right are run with the axial and vector pole masses taken to infinity.

Fig. 14 shows the result of transforming from q^2 to z according to the Hill prescription[9]. Over the very narrow $-z$ range accessible for $D^+ \to K^- \pi^+ \ell^+ \nu$, it is not surprising that that the transformed form factor is essentially constant.

It is interesting to note that the FOCUS analysis was based on a sample of 11400 $D^+ \to K^- \pi^+ \mu^+ \nu$ events, while the CLEO analysis was based on a sample of only 2470 $D^+ \to K^- \pi^+ e^+ \nu$ events. The error bars in Fig. 14 for FOCUS data are much larger than those for the much smaller CLEO data set and only four FOCUS q^2 bins are reported on. This is because of the much poorer q^2 resolution in fixed target semileptonic decay compared to the order-of-magnitude better q^2 resolution obtainable for semileptonic analyses in charm threshold data from e^+e^- colliders where the neutrino can be reconstructed using energy-momentum balance. This is especially relevant for $D^+ \to K^- \pi^+ \ell^+ \nu$ since the 1 GeV^2 q^2 range for $D^+ \to K^- \pi^+ \ell^+ \nu$ is a factor of two smaller than that in $D^0 \to K^- \ell^+ \nu$. Error inflation due to deconvolution grows dramatically once the bin-to-bin separation, Δq^2, approaches the r.m.s. resolution, $\sigma(q^2)$, which was typically 0.18 GeV^2 in the four bins reported on by FOCUS[13].

What can we learn about the phase of the s-wave contribution? Recall in Figure 8 the asymmetry created by the interference between the s-wave and $D^+ \to \overline{K}^{*0} \ell^+ \nu_\ell$ only appeared below the $\overline{K}^{*0}$ pole in FOCUS data and thus the s-wave phase was such that
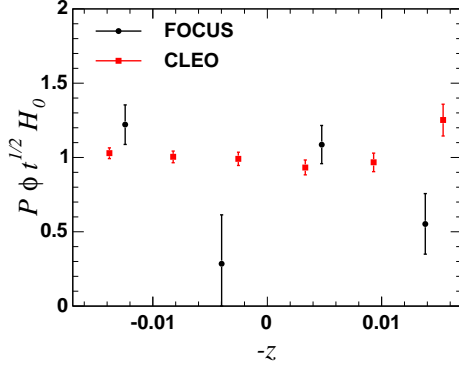
FIG. 14: Transformation of $H_0(q^2)$ into $H_0(z)$ by R.J. Hill[9]. Here $t \equiv q^2$ and P and ϕ are functions of q^2 designed to remove the simple poles. The FOCUS data is from Reference [13] and the CLEO data is from Reference [3].

it was orthogonal with the $m_{K\pi} > m(\overline{K}^{*0})$ half of the Breit-Wigner amplitude or $\langle BW_+ \rangle$. Since the asymmetry is "negative" according to the convention of Eq. (5), in that favors the backward over the forward $\cos\theta_V$ direction, it must be anti-collinear to $\langle BW_- \rangle$ as well. Hence it must have roughly the phase of 40^0 as illustrated by Fig. 15. FOCUS[14] measured the s-wave phase to be $\delta = (39 \pm 4 \pm 3)^0$.
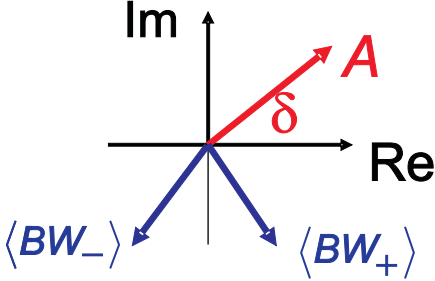

FIG. 15: Illustration of s-wave phase

As Figure 16 shows, the same thing happens in CLEO data. The effective $h_0(q^2)\,H_0(q^2)$ disappears above the $\overline{K}^{*0}$ pole and is very strong below the pole. The amplitude A of the s-wave piece is arbitrary since using interference we can only observe the product $A\,H_0(q^2)\,h_0(q^2)$. This means any change in A scale can be compensated by a change of scale in $h_0(q^2)$. The fact that the $h_0(q^2)\,H_0(q^2)$ data was a tolerable match (at least in the low q^2 region) to the FOCUS curve in Figure 11 does imply, however, that the s-wave amplitude observed in CLEO is consistent with that of FOCUS. A more formal fit of the s-wave parameters in CLEO data is in progress.
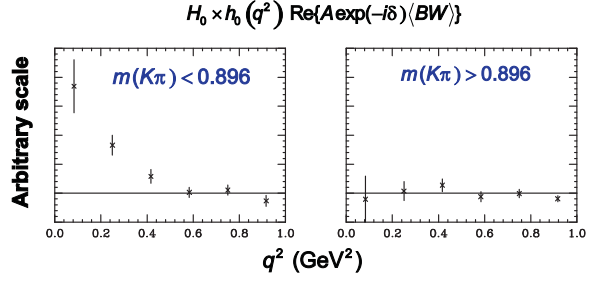

FIG. 16: The s-wave interference term for events below the $\overline{K}^{*0}$ pole (left) and above the pole (right). The interference term depends on the s-wave phase relative to the phase average phase of each half of the Breit-Wigner. All of the $\cos\theta_V$ interference observed by FOCUS was also below the $\overline{K}^{*0}$ pole as shown in Fig. 8

Finally, is there evidence for higher $K^-\pi^+$ angular momentum amplitudes in $D^+ \to K^-\pi^+\ell^+\nu$? We searched for possible additional interference terms such as a (zero helicity) d-wave contribution: $4\sin^2\theta_\ell(3\cos^2\theta_V - 1)\,H_0(q^2)\,h_0^{(d)}(q^2)\,\mathrm{Re}\{Ae^{-i\delta}\mathrm{BW}\}$ or an f-wave contribution: $4\sin^2\theta_\ell\cos\theta_V(5\cos^2\theta_V - 3)\,H_0(q^2)\,h_0^{(f)}(q^2)\,\mathrm{Re}\{Ae^{-i\delta}\mathrm{BW}\}$. As shown in Figure 17, there is no evidence for such additional contributions which should diverge as $1/q^2$ at low q^2.
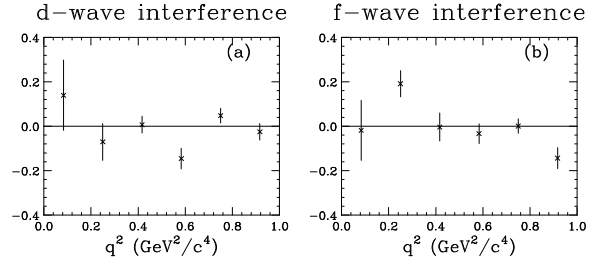

FIG. 17: Search for (a) d-wave and (b) f-wave interference effects as described in the text.

VI. FUTURE DIRECTIONS

It will be interesting to pursue the non-parametric $D^+ \to K^-\pi^+\ell^+\nu$ analysis with more data. One motivation is will be to further study the $h_0(q^2)$ form factor which appears to be somewhat different than $H_0(q^2)$. It would also be interesting to pursue tighter limits on possible d-wave and f-wave non-resonant contributions to $D^+ \to K^-\pi^+\ell^+\nu$ and make more stringent tests of SPD. CLEO is slated to increase their luminosity at the $\psi(3770)$ from the 280 pb^{-1} reported here to 750 pb^{-1}. In addition Surik Mehrabyan and I, are studying $D^+ \to K^-\pi^+\mu^+\nu$ as well as $D^+ \to K^-\pi^+e^+\nu$ in CLEO data. This is a some-

what challenging project since the CLEO muon detector was designed for higher energy B-meson running and the muons from charm semileptonic decay tend to range out before being identified. Hence special care must be exercised to reduce backgrounds. Besides increasing our statistics, the $D^+ \to K^-\pi^+\mu^+\nu$ should allow us to make the first measurements of the $H_T(q^2)$ form factor which is suppressed by a factor of m_ℓ^2/q^2. Since this is a zero helicity factor, it can interfere with $H_0(q^2)$ and hence two new projectors will be required: one for the $H_T^2(q^2)$ term and one for $H_0(q^2) \times H_T(q^2)$ interference. At present the prognosis for making these measurements looks good.

VII. SUMMARY

Progress in understanding $D \to$ vector $\ell^+\nu$ decays was reviewed. These have historically been an-

alyzed under the assumption of spectroscopic pole dominance (SPD). A recent result from BaBar was reviewed that used SPD to show that the form factors for $D_s^+ \to \phi\, \ell^+\nu_\ell$ are consistent with those from $D^+ \to K^-\pi^+\ell^+\nu$ as expected from SU(3) symmetry. Experiments have obtained consistent results with the SPD assumption, but as of yet there have been no incisive tests of spectroscopic pole dominance. We concluded by describing a first non-parametric look at the $D^+ \to K^-\pi^+\ell^+\nu$ form factors. Although the results were very consistent with the traditional pole dominance fits, the data was not precise enough to incisively measure q^2 dependence of the axial and vector form factors and thus test SPD. This preliminary analysis did confirm the existence of an s-wave effect first observed by FOCUS [1], but was unable to obtain evidence for d and f-waves.

[1] FOCUS Collaboration, J.M. Link et al., Phys. Lett. B **535**, 43 (2002).

[2] The BaBar Collaboration, B.Aubert et al., Submitted to the 33rd International Conference on High-Energy Physics, ICHEP 06, 26 July- 2 Aug 2006, Moscow, Russia, hep-ex/0607085 (2006)

[3] CLEO Collab., Phys. Rev. D**74**, (2006) 052001.

[4] J. Wiss, "Recent Results on Fully Leptonic and Semileptonic Charm Decays", FPCP 2006, Vancouver, Canada, hep-ex/0605030 (2006)FPCP

[5] J.G. Korner and G.A. Schuler, Z. Phys. C **46**, 93 (1990).

[6] FOCUS Collaboration, J.M. Link et al., Phys. Lett. B **586**, 183 (2004).

[7] D.Becirevic and A. Kaidalov, Phys. Lett. B**478** , 417-423(2000)

[8] S. Fajfer and J. Kamenik, Phys. Rev. D **72**, 034029 (2005).

[9] Richard J. Hill, "The Modern Description of Semileptonic Form Factors", FPCP 2006, Vancouver, Canada, hep-ex/0606023 (2006)FPCP

[10] Richard J. Hill, Phys.Rev. D**73** (2006) 014012

[11] FOCUS Collaboration, J.M. Link et al., Phys. Lett. B**648** 156-163 (2007).

[12] FOCUS Collaboration, J.M. Link et al., Phys. Lett. B**653** 1-11 (2007).

[13] FOCUS Collaboration, J.M. Link et al., Phys. Lett. B **633**, 183 (2006).

[14] FOCUS Collaboration, J.M. Link et al., Phys. Lett. B **544**, 89 (2002).